Journal of Southeast University (English Edition) Vol. 42, No. 2, pp. 233-239 June 2026 ISSN 1003-7985

Water film depth of super-multi-lane pavement and its effect on tire-pavement surface interaction

CHEN Jun[1], LIAO Bing[1], ZHOU Lailiang[1], DONG Zhenhai[2], SI Xiufen[2], ZHOU Yan[2]

(1. College of Civil and Transportation Engineering, Hohai University, Nanjing 210098, China;
2. STECOL Corporation, Tianjin 300392, China)

Abstract: To investigate the water film depth (WFD) of super-multi-lane (SML) pavement and its effect on tire-pavement surface interaction, a rainfall-runoff model of SML pavement was developed, and the influence of the number of lanes and pavement slopes was analyzed. Based on the realistic texture of pavement surface, a tire-pavement surface-water film coupling model was established. The contact characteristics between the tire and the pavement surface, as well as the critical hydroplaning speeds under different WFDs, were analyzed. The results show that the WFD of the pavement increases significantly with the increase in lane number. Pavement expanding from three to five lanes in a single direction has the largest increase of the WFD, while the increment decreases as the number of lanes further increases. Increasing the transverse slope from 1.5% to 2.0% results in the most obvious decrease in the WFD. Moreover, increasing the longitudinal pavement slope to 1.0%-2.0% significantly reduces the area of thick water film on the pavement surface. The higher WFD results in a more rapid decrease in the tire-pavement surface contact force as the vehicle speed rises, leading to a lower critical hydroplaning speed. The critical hydroplaning speed of the vehicle decreases by approximately 6 km/h for every 2 mm increase in the WFD.

Key words: water film depth (WFD); lane number; pavement slope; tire-pavement; critical hydroplaning speed

DOI: 10.3969/j.issn.1003-7985.2026.02.010

With the increase in traffic volume in many heavily traveled countries, the number of super-multi-lane (SML) expressways (two-way, eight-lane or more) has risen sharply [1-2]. Although the widening of expressways has greatly eased traffic congestion pressure, it has also exacerbated a series of driving safety problems. One of the problems is the significant increase in hydroplaning risks on rainy days due to the thicker water film on outer lanes of SML expressways, which is caused by their wider pavements[3-4]. The squeezing between the water film and the tire generates hydrodynamic pressure, resulting in a reduction of the contact area and friction between the tire and the pavement[5-6]. The thicker the water film, the more significant the reduction in friction coefficient between the tire and the pavement [7-9]. Therefore, it is essential to examine the water film depth (WFD) of SML pavement and its impact on the interaction between the tire and the pavement.

Presently, there are two general methods for WFD prediction: empirical formulas and theoretical models. Researchers have established the relationship between WFD and its influencing factors through empirical regression and have developed empirical formulas[10-12]. Since the empirical formulas use field test data based on local rainfall intensity and pavement material to predict the WFD, their application is limited to specific conditions[13-14]. Considering the limitations of empirical formulas, researchers have developed more universal theoretical models for WFD prediction using fluid mechanics principles. However, most theoretical models oversimplify runoff and are derived according to specific requirements[15], leading to predictions that deviate from actual results. Therefore, the existing WFD prediction methods are not suitable for the WFD calculation of SML expressways.

Numerous tire-pavement interaction models have been developed to investigate the contact between the tire and the pavement, such as the widely used Penn State friction model, PIARC friction model and Pacejka friction model[16]. In addition, the evolving understanding of tire-pavement interaction has revealed the important influence of water film[17-19] and pavement texture[20-22] on this interaction. Kane et al. [23] established a regression model to characterize the connection of the WFD, friction, and microtexture. Tang et al. [24] used the Euler-Lagrange method to analyze the interaction mechanism between the tire, water, and pavement in terms of microscopic texture. However, previous studies have tended to use simplified methods to construct pavement textures, such as employing lower friction coefficients to directly represent pavement texture.

In this study, a rainfall-runoff model of SML pave-

Received 2025-07-09, **Revised** 2025-09-30.

Biography: CHEN Jun (1981—), male, doctor, professor, chen_jun2728@163.com.

Foundation item: The National Natural Science Foundation of China (No. 52178421).

Citation: CHEN Jun, LIAO Bing, ZHOU Lailiang, et al. Water film depth of super-multi-lane pavement and its effect on tire-pavement surface interaction[J]. Journal of Southeast University (English Edition), 2026, 42(2): 233-239. DOI: 10.3969/j.issn.1003-7985.2026.02.010.

ment was constructed and validated against some previous WFD prediction formulas. The effects of lane number and pavement slope on the WFD under different rainfall intensities were analyzed. Furthermore, to investigate the influences of the WFD on the interaction between the tire and the pavement, a tire-pavement surface-water film coupling model considering the realistic texture was constructed. Based on the WFD on SML pavement, the changes in tire-pavement contact force with vehicle speed under different WFDs were simulated.

1 WFD Simulation of SML Pavement

1.1 Rainfall-runoff model

A right-half pavement model spanning 50 m in length with lanes each measuring 3.75 m in width was constructed. Since the rainfall intensity and the falling speed of raindrops can be defined by specific parameters, the vertical height of the model exerts minimal influence on the simulation results. Through iterative trial computations, the computational domain was situated 1 m above the pavement surface. The upper and side areas of the pavement model were designated as velocity inlets (1 m/s) and pressure outlets, representing rainfall and drainage dispersion, respectively. The initial gauge pressures at both the inlet and outlet of the model were set at 0 Pa.

The rainfall process was simulated using the discrete-phase model (DPM), which tracks the trajectories of discrete-phase particles (raindrops). The force equilibrium equation for particles in the Cartesian coordinate system is shown as

$$\frac{du_p}{dt} = F_D(u - u_p) + \frac{g_x(\rho_p - \rho)}{\rho_p} + F_x \qquad (1)$$

where u_p is the velocity of raindrops, m/s; t is the time, s; F_D is the drag force of raindrops, N; u is the velocity of air, m/s; g_x is the gravitational acceleration, m/s^2; ρ_p and ρ are the densities of raindrops and air, respectively, m/s^2; F_x is the other force on the raindrops, N.

The Euler wall film model was employed to capture the DPM raindrop particles and to simulate the flow of water. The mass conservation equation of two-dimensional (2D) liquid films in the three-dimensional (3D) domain is shown as

$$\frac{\partial \rho_l h}{\partial t} + \nabla_s(\rho_l h V_l) = \dot{m}_s \qquad (2)$$

where ρ_l is the water density, g/cm^3; h is the water film height, mm; ∇_s is the surface gradient operator; V_l is the vector of average film velocity, m/s; $\dot{m}_s$ is the mass source term per unit area for the water film, g/cm^2.

1.2 Simulation validation

The reliability of this simulation was validated against empirical formulas by Refs. [10-12]. The WFDs were simulated with a rainfall intensity R of 1 mm/min, a transverse slope S_T of 1.5%, and a longitudinal slope S_L of 2.0%, as shown in Fig. 1. The simulated values fall within the range established by the empirical formulas from Refs. [10, 12] and have a good correlation with that from Ref. [12]. In addition, the WFD simulation results exhibit a consistent overall trend with the three empirical formulas, indicating a nonlinear increase in the WFD with greater drainage length, which supports the rationality of the simulation.

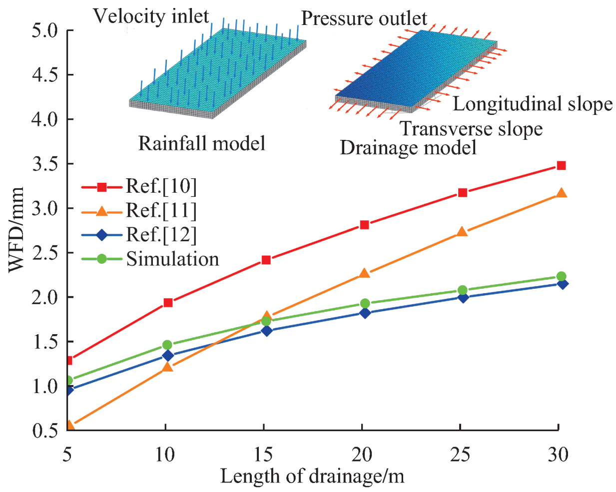

Fig. 1 WFDs of pavement with different drainage lengths

2 Factors Affecting Pavement WFD

2.1 Number of pavement lanes

According to the Specifications for Drainage Design of Highway (JTG/T D33—2012), the slope drainage design within the pavement boundary should be in accordance with the 15-year recurrence period standard. Taking Nanjing as an example, the rainfall intensity for a 5 min duration with a 15-year return period is 3.175 mm/min. Therefore, the rainfall intensity was set from 1 to 4 mm/min.

When the transverse slope and longitudinal slope of pavement are set at 2.0% and 0.5% respectively, the WFDs across the transverse direction of each lane under different rainfall intensities are shown in Fig. 2. The WFD demonstrates a positive correlation with pavement width under different rainfall intensities. In addition, with an increase in the number of lanes, the increment rate of the WFD slows down, and the WFD reaches a plateau in the seventh lane.

Fig. 3 shows the maximum WFDs under identical rainfall intensities for 6-, 10- and 14-lane pavements, demonstrating the effect of pavement widening on the WFD. At a rainfall intensity of 1 mm/min, widening the same number of lanes on pavements with different initial lane counts yields nearly identical increments in the WFD for each pavement. However, at rainfall intensities of 2 mm/min and higher, widening the half-width pavement

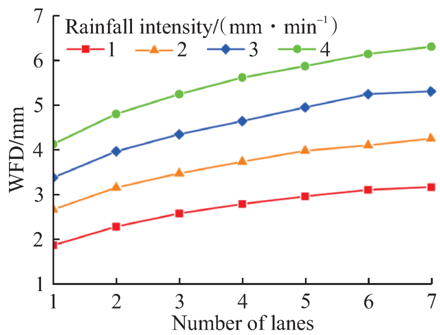

Fig. 2 WFDs on each lane under different rainfall intensities

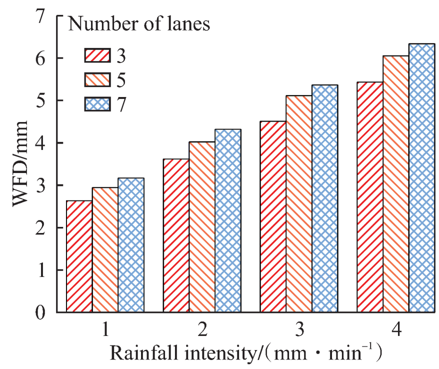

Fig. 3 Maximum WFDs for pavements with different numbers of lanes

from three to five lanes results in a more pronounced increase in WFD compared to widening it from five to seven lanes. The results indicate that augmenting the number of lanes results in a significant increase in maximum WFD for the pavements with fewer initial lanes. Conversely, further increases in the number of lanes yield a more modest increase in WFD for pavements with a greater initial number of lanes.

2.2 Pavement slope

Fig. 4 shows the WFDs of pavements with different slopes under a rainfall intensity of 1 mm/min. The WFD consistently diminishes as the transverse slope of the pavement increases. The increase in the transverse slope of pavement from 1.5% to 3.0% results in an approximate 13.0% reduction in WFD. Notably, the most significant decrease in WFD occurs when the transverse slope is raised from 1.5% to 2.0%, particularly noted in the third to fifth lanes. Moreover, the increase in the longitudinal slope has only a marginal impact on the maximum WFD, with merely an approximate 3.0% increase observed as the longitudinal slope of the pavement progresses from 1.5% to 3.0%.

To further investigate the influence of pavement longitudinal slope on WFD, Fig. 5 illustrates the drainage paths and WFDs of pavement with a transverse slope of 2% under different longitudinal slopes. The flow paths of the water on the pavement align with the synthetic slope direction. As the longitudinal slope increases, the

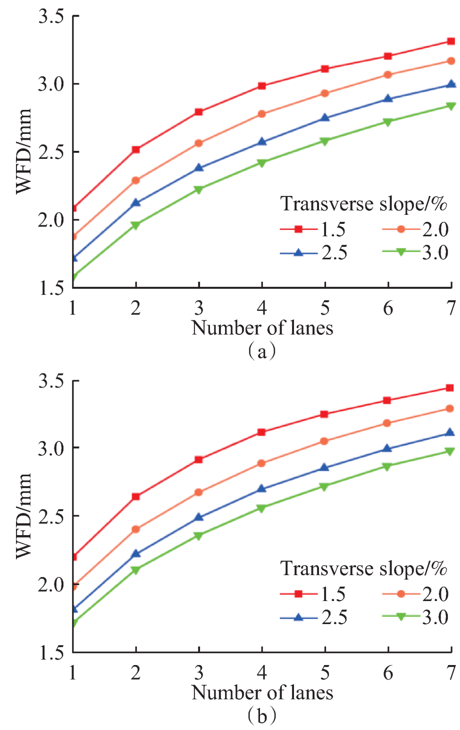

Fig. 4 WFDs of pavements with different slopes. (a) S_L = 0.5%; (b) S_L = 3.0%

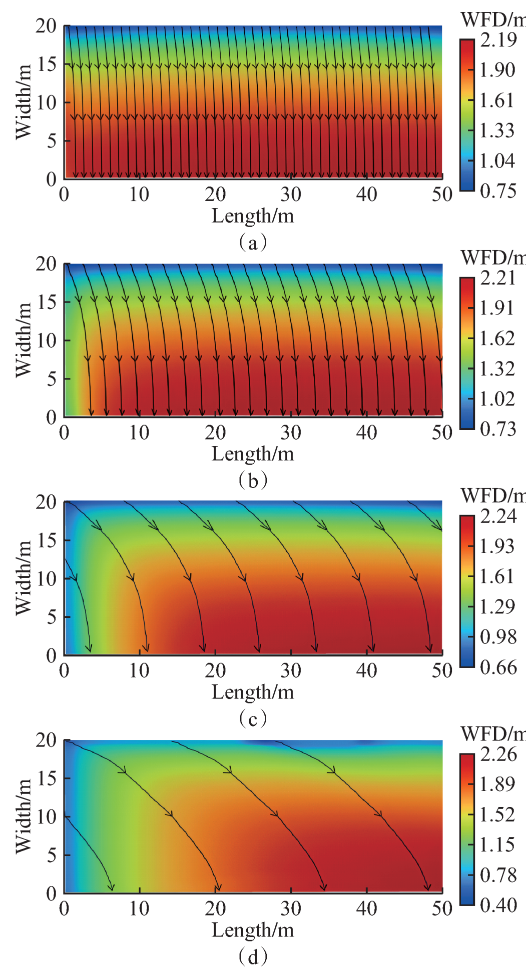

Fig. 5 Drainage paths and WFDs of pavement with different longitudinal slopes. (a) S_L = 0.5%; (b) S_L = 1.0%; (c) S_L = 2.0%; (d) S_L = 3.0%

flow path of water on pavement elongates, leading to a marginal rise in the maximum WFD. Moreover, the thick water film exhibits uniform distribution on the outside of the pavement for minor longitudinal pavement slopes. However, the higher longitudinal slopes concentrate the thick water film predominantly in the downstream section on the outside of the pavement. Consequently, a moderate increase in the longitudinal slope (1.0% to 2.0%) is advantageous for minimizing the distribution area of thick water film on pavement, while the corresponding increase in the maximum WFD remains negligible.

3 Effect of WFD on Tire-Pavement Surface Interaction

Different rainfall intensities and pavement slopes lead to the formation of water films with different depths on each lane of the pavement. To further investigate the effect of WFD on the tire-pavement surface contact, a tire-pavement surface-water film coupling model was constructed, and the tire-pavement contact forces under different vehicle speeds and WFDs were simulated.

3.1 Tire-pavement surface-water film coupling model

3.1.1 Tire model

The 2D finite-element model of the tire was established using 205/55R16 radial tires. The cross-sectional width, tread width, and outer diameter of the tire are 205, 172, and 628 mm, respectively. The parameters and specifications of the tire skeleton components are shown in Table 1. The 2D tire model was rotated around the neutral axis by 360° to generate the 3D tire model based on the rotational symmetry of the 3D tire model, as shown in Fig. 6.

Table 1 Parameters and specifications of tire skeleton components

Component	Elasticity modulus/GPa	Poisson ratio	Density/($kg \cdot m^{-3}$)	Spacing/mm	Angle/(°)	Cross-sectional area/mm^2
Belt ply 1	205.00	0.3	7 430	1.43	63	0.21
Belt ply 2	205.00	0.3	7 430	1.43	117	0.21
Carcass ply	105.49	0.3	8 190	0.90	0	0.24
Cap ply	223.00	0.3	7 590	1.37	90	0.21
Bead wire	170.00	0.3	12 370	1.05	90	0.69

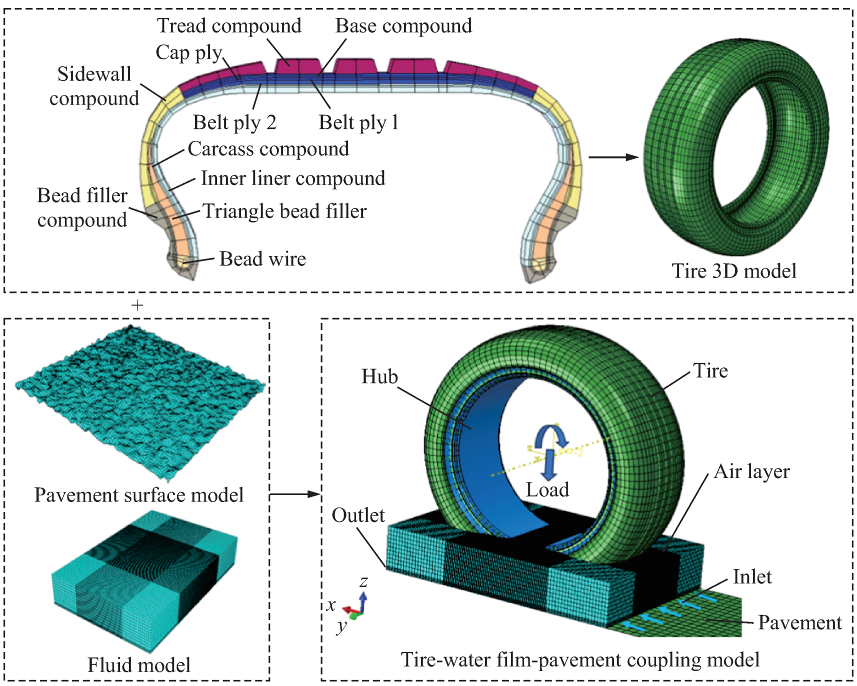

Fig. 6 Tire-pavement surface-water film coupling model

3.1.2 Pavement surface model and fluid model

The AC with a normal maximum aggregate size of 13.2 mm (AC-13) was designed with styrene-butadiene-styrene modified asphalt, limestone mineral powder and crushed basalt aggregate. The aggregate gradation of AC-13 is shown in Table 2. The asphalt content of AC-13 is determined to be 5.1%. The surface images of the AC-13 slab were captured from various angles using a camera, followed by a series of processing steps that included segmentation, correction, and noise reduction. The processed images were subsequently imported into the VisualSFM platform, where surface feature point

Table 2 Aggregate gradation of AC-13

Sieve size/mm	16	13.2	9.5	4.75	2.36	1.18	0.6	0.3	0.15	0.075
Passing ratio/%	100	96.5	76.0	57.2	33.6	26.5	20.2	13.5	10.3	7.2

data was extracted employing the SURF algorithm to generate the 3D dense point cloud file. Then, the point cloud file was imported into COMSOL to obtain the 3D pavement surface model. As shown in Fig. 6, the fluid model on the pavement surface consists of a water film layer and an air layer (600 mm × 400 mm × 110 mm). The number of air layer grids is 158 080, the number of water film layer grids is 63 232, and the Euler element type is EC3D8R.

3.1.3 Tire-pavement surface-water film coupling

The tire-pavement surface-water film model is constructed by coupling the tire model, pavement surface model and fluid model, as shown in Fig. 6. The tire was embedded in the fluid domain and contacted the upper part of the pavement surface. The tire-water film interaction was governed by Eulerian-Lagrangian contact, which calculates the hydrodynamic pressure exerted by the water flow on the tire tread. The lower boundary of the fluid model was designed to completely fit the upper part of the pavement surface to maintain a consistent WFD. In the simulation process, the tire rolls in place as a deformable body, while the water flow and the pavement surface move toward the tire at a translational speed equivalent to the vehicle velocity.

3.2 Effect of WFD on tire-pavement surface interaction

The accelerated movement process of the pavement surface with a 10 mm water film toward the tire from 40 to 100 km/h at an acceleration of 2 m/s^2 was simulated based on the tire-pavement surface-water film coupling model. Fig. 7 shows the water film states and the tire-pavement surface contact areas at speeds of 40, 60, 80, and 100 km/h. With the increase in speed, the water between the tire and the pavement surface flows and converges along the lateral direction of the tire under the tire's squeezing, forming a relatively thick water wedge on both sides of the tire. This is because, at high speeds, the water between the tire and the pavement surface can not be discharged through the tire grooves in time. In addition, the tire-pavement surface contact area decreases gradually as speed increases. The tire almost completely loses contact with the pavement surface when the vehicle reaches a speed of 100 km/h.

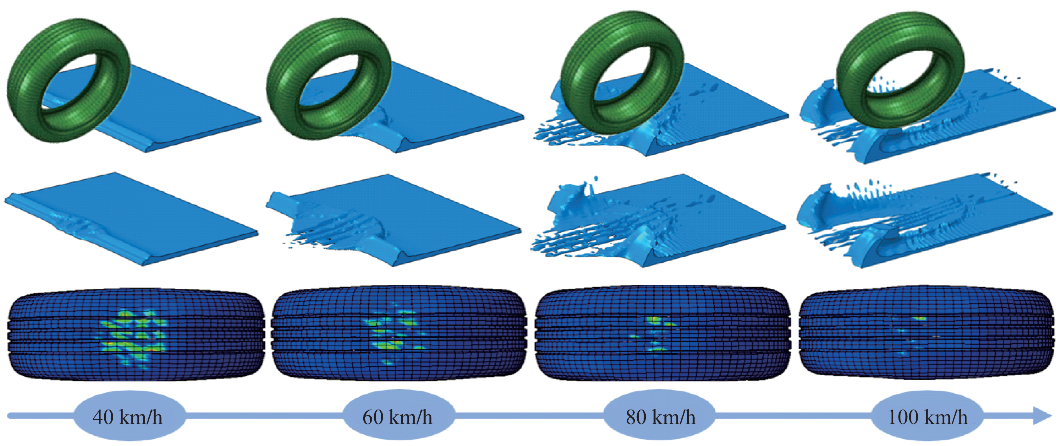

Fig. 7 Water film states and tire-pavement surface contact areas

Fig. 8 demonstrates the variation in tire-pavement surface contact force at different WFDs with a tire inflation pressure of 0.23 MPa and a tire load of 4 kN. The contact force between the tire and the pavement surface decreases as the vehicle speed increases, ultimately reaching zero at the critical hydroplaning speed. The higher WFD results in a more rapid decline in the tire-pavement surface contact force as vehicle speed rises, leading to a lower critical hydroplaning speed. Specifically, for the WFDs of 2, 4, 6, and 8 mm, the corresponding critical hydroplaning speeds of the vehicle are 131, 123, 117, and 111 km/h, respectively. Thus, the critical hydro-

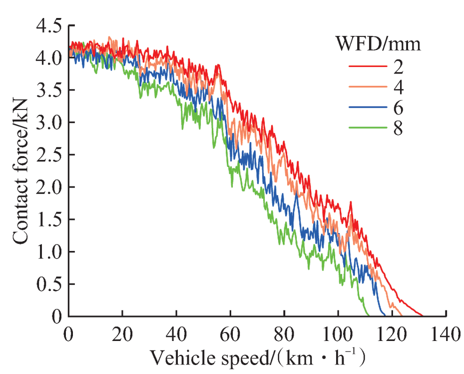

Fig. 8 Tire-pavement surface contact force under different WFDs

planing speed of the tire decreases by approximately 6 km/h for every 2 mm increase in the WFD.

Based on WFD simulation, the maximum WFD for each lane ranges from 2 to 6. 5 mm under rainfall intensities from 1 to 4 mm/min, with the transverse and longitudinal slopes of pavement set at 2. 0% and 0. 5%, respectively. Specifically, the WFDs of 2, 4, 6, and 8 mm correspond to the first lane at a rainfall intensity of 1 mm/min, the seventh lane at 2 mm/min, the seventh lane at 4 mm/min, and higher rainfall conditions, respectively. Therefore, to ensure driving safety on rainy days, it is advisable to control the transverse slope of the SML expressway within the range of 1. 5% to 2. 0% and the longitudinal slope within 1. 0%-2. 0% to reduce the WFD. When the rainfall intensity is 2-4 mm/min, it is recommended that the vehicle try to drive on the inside three lanes of pavement.

4 Conclusions

(1) With the increase in the number of lanes, the WFD increases correspondingly, while its growth rate decreases gradually and tends to level off at the seventh lane. The largest increase in the WFD is observed when expanding a half-width pavement from three to five lanes.

(2) The increase in the transverse slope of the pavement from 1. 5% to 2. 0% leads to the most significant reduction in the WFD, with the extent of reduction gradually decreasing as the transverse slope increases. Increasing the longitudinal slope to 1. 0%-2. 0% reduces the distribution area of thick water film on the pavement.

(3) As the vehicle speed increases, a thicker water wedge forms on both sides of the tire and the tire-pavement surface contact area gradually decreases.

(4) The higher WFD results in a more rapid decline in the tire-pavement surface contact force as vehicle speed rises, leading to a lower critical hydroplaning speed. The critical hydroplaning speed of the vehicle decreases by approximately 6 km/h for every 2 mm increase in the WFD.

References

[1] WEI X Y, XU C C, WANG W, et al. Capacity analysis and model development of the multilane freeway [J]. Journal of Transportation Systems Engineering & Information Technology, 2017, 17(2): 105-111. (in Chinese)

[2] DAN H C, GAO L S, WANG H, et al. Discrete-element modeling of mean texture depth and wearing behavior of asphalt mixture[J]. Journal of Materials in Civil Engineering, 2022, 34(4): 04022027.

[3] SPITZHÜTTL F, GOIZET F, UNGER T, et al. The real impact of full hydroplaning on driving safety[J]. Accident Analysis & Prevention, 2020, 138: 105458.

[4] LI Q, WANG J Q, LU Y, et al. Effect of dynamic water pressure on the adhesion behavior of recycled asphalt-aggregate interface by molecular dynamics method[J]. Construction and Building Materials, 2023, 382: 131296.

[5] XIAO K, HUI B, QU X, et al. Asphalt pavement water film thickness detection and prediction model: A review [J]. Journal of Traffic and Transportation Engineering (English Edition), 2023, 10(3): 349-367.

[6] ZHAO K, ZHOU Q, ZHAO E Q, et al. A new water film depth prediction model for pavement surface drainage[J]. Infrastructures, 2024, 9(3): 36.

[7] PENG J, CHU L, FWA T F. Determination of safe vehicle speeds on wet horizontal pavement curves [J]. Road Materials and Pavement Design, 2021, 22(11): 2641-2653.

[8] CHEN X B, WANG J T, LIU H, et al. Influence of rainfall on skid resistance performance and driving safety conditions of asphalt pavements[J]. Journal of Southeast University (English Edition), 2019, 35(4): 482-490.

[9] HE J, CHEN H Z, FANG Z M, et al. Analysis on research status and development trends of vehicle stability control on low-adhesion road surfaces [J]. Journal of Southeast University (Natural Science Edition), 2025 [2025-07-10]. http://kns. cnki. net/kcms/detail/32. 1178. N. 20250609. 1426. 004. html. (in Chinese)

[10] GALLAWAY B M, SCHILLER R E, ROSE J G. The effects of rainfall intensity, pavement cross slope, surface texture, and drainage length on pavement water depths [R]. College Station, TX, USA: Texas A&M University, 1971.

[11] JI T J, HUANG X M, LIU Q Q, et al. Prediction model of rain water depth on road surface[J]. Journal of Traffic and Transportation Engineering, 2004, 4(3): 1-3. (in Chinese)

[12] LUO J, LIU J B, WANG Y Q. Validation test on pavement water film depth prediction model[J]. China Journal of Highway and Transport, 2015, 28(12): 57-63. (in Chinese)

[13] LING J M, YANG F, ZHANG J K, et al. Water-film depth assessment for pavements of roads and airport runways: A review[J]. Construction and Building Materials, 2023, 392: 123054.

[14] LUO W T, WANG K C P, LI L. Field test validation of water film depth (WFD) prediction models for pavement surface drainage[J]. International Journal of Pavement Engineering, 2019, 20(10): 1170-1181.

[15] MA Y L, GENG Y F, CHEN X H, et al. Prediction for asphalt pavement water film thickness based on artificial neural network [J]. Journal of Southeast University (English Edition), 2017, 33: 490-495.

[16] ZHAO L R, ZHAO H D, CAI J W. Tire-pavement friction modeling considering pavement texture and water film[J]. International Journal of Transportation Science and Technology, 2024, 14: 99-109.

[17] CHEN X, WANG H. Analysis and mitigation of hydroplaning risk considering spatial-temporal water condition on the pavement surface [J]. International Journal of Pavement Engineering, 2023, 24(2): 2036988.

[18] DONG P J, CAO X J, TANG B M. Research on the dy-

namic response characteristics of asphalt pavement under hydro-thermo-mechanical coupling[J]. Journal of Southeast University (Natural Science Edition), 2025, 55(4): 1001-0505. (in Chinese)
[19] ZHAN Y, TANG B, ZOU Y W, et al. Analysis of pavement adhesion coefficient under rainy conditions based on tire-road coupled hydroplaning mechanism[J]. Journal of Southeast University (Natural Science Edition), 2026, 56(2): 251-258. (in Chinese)
[20] GONG Z L, MIAO Y H, LANTIERI C. Review of research on tire-pavement contact behavior[J]. Coatings, 2024, 14(2): 157.
[21] GONG Z L, MIAO Y H, LI W, et al. Analysis of tyre-pavement contact behaviour of heavy truck in full-scale test[J]. International Journal of Pavement Engineering, 2023, 24(1): 2235630.
[22] HUANG X M, SUN Y T, XU H C, et al. Analysis on texture characteristics of positive texture skid-resistance friction course based on discrete element[J]. Journal of Southeast University (Natural Science Edition), 2024, 54(6): 1520-1529. (in Chinese)
[23] KANE M, DO M T, CEREZO V, et al. Contribution to pavement friction modelling: An introduction of the wetting effect[J]. International Journal of Pavement Engineering, 2019, 20(8): 965-976.
[24] TANG T C, ANUPAM K, KASBERGEN C, et al. A finite element study of rain intensity on skid resistance for permeable asphalt concrete mixes[J]. Construction and Building Materials, 2019, 220: 464-475.

超多车道路面水膜厚度及其对轮胎-路表相互作用的影响

陈俊[1], 廖兵[1], 周来良[1], 董振海[2], 司秀芬[2], 周岩[2]

(1.河海大学土木与交通学院,南京 210098;2.中国电建市政建设集团有限公司,天津 300392)

摘要: 为研究超多车道(SML)路面水膜厚度(WFD)及其对轮胎-路表相互作用的影响,构建了SML路面的降雨汇流模型,分析了车道数和路面坡度对WFD的影响。基于路表真实纹理,建立了轮胎-路表-水膜耦合模型,分析了不同WFD下轮胎与路表接触特征及轮胎临界滑水速度。结果表明,随路表车道数的增多,路表水膜厚度显著增大。当路面从半幅3车道拓宽至5车道时,WFD增加最显著,但其增量随车道数进一步增加而逐渐减小。当路面横坡从1.5%增至2.0%时,WFD降低幅度最大。将路面纵坡增加至1.0%~2.0%,路表较厚水膜的分布面积明显减少。WFD越大,胎-路间接触力随车速增加而下降得越快,导致临界滑水速度越小。WFD每增加2 mm,车辆临界滑水速度下降约6 km/h。

关键词: 水膜厚度(WFD);车道数;路面坡度;轮胎-路表;临界滑水速度

中图分类号: U414